

Development of a novel 3-degrees of freedom flexure based positioning system

Hyo-Young Kim, Da-Hoon Ahn, and Dae-Gab Gweon

Citation: *Rev. Sci. Instrum.* **83**, 055114 (2012); doi: 10.1063/1.4720410

View online: <http://dx.doi.org/10.1063/1.4720410>

View Table of Contents: <http://rsi.aip.org/resource/1/RSINAK/v83/i5>

Published by the [American Institute of Physics](#).

Related Articles

Experimental investigation effects of blend hazelnut oil on compression ignition engine performance characteristics and emission

J. Renewable Sustainable Energy **4**, 042701 (2012)

Graphene radio: Detecting radiowaves with a single atom sheet

Appl. Phys. Lett. **101**, 033109 (2012)

Metallic glass mold insert for hot embossing of polymers

J. Appl. Phys. **112**, 024506 (2012)

A probabilistic model for the identification of confinement regimes and edge localized mode behavior, with implications to scaling laws

Rev. Sci. Instrum. **83**, 10D715 (2012)

The low-carbon transformation—A social science perspective

J. Renewable Sustainable Energy **4**, 041404 (2012)

Additional information on *Rev. Sci. Instrum.*

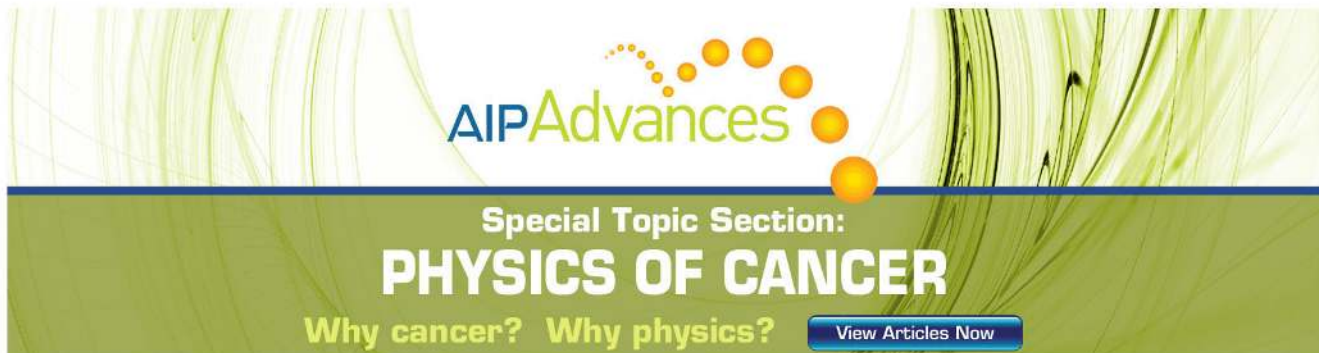
Journal Homepage: <http://rsi.aip.org>

Journal Information: http://rsi.aip.org/about/about_the_journal

Top downloads: http://rsi.aip.org/features/most_downloaded

Information for Authors: <http://rsi.aip.org/authors>

ADVERTISEMENT



AIP Advances

Special Topic Section:
PHYSICS OF CANCER

Why cancer? Why physics? [View Articles Now](#)

Development of a novel 3-degrees of freedom flexure based positioning system

Hyo-Young Kim,^{a)} Da-Hoon Ahn, and Dae-Gab Gweon
Mechanical Engineering Department, KAIST, Daejeon, Korea

(Received 9 February 2012; accepted 7 May 2012; published online 29 May 2012)

Flexure mechanisms have been widely used for nanometer positioning systems. This article presents a novel conceptual design of an ultra-precision 3-degrees of freedom ($XY\theta_Z$) positioning system with nanometer precision. The main purpose of this novel stage design is for the application of measurement equipment, in particular biological specimens. The stage was designed as a hollow type and with a compact size for the inverted microscope. This stage includes piezoelectric transducer actuators, double compound amplification mechanisms, moving plate, and capacitor sensors. The double compound amplification mechanism was designed using a mathematical model and analyzed by the finite element method. Since the relationship between the variables of the hinge parameters and system performances are complicated, an optimization procedure was used to obtain the optimal design parameters, which maximized the system bandwidth. Based on the solution of the optimization problem, the design of the stage and FEM simulation results are presented. Finally, the stage was manufactured and tested. © 2012 American Institute of Physics. [<http://dx.doi.org/10.1063/1.4720410>]

I. INTRODUCTION

A. Motivation

Precision nano-positioning techniques have become very important for biomedical science, optics, and microscopy. Piezoelectric transducer (PZT) and flexure mechanisms are widely used in these various fields and applications within these fields. Flexure mechanisms are flexible structures, which can generate the desired motions by undergoing elastic deformation instead of through rigid linkage/joints as in rigid body mechanisms.¹⁻³ The advantages of flexure mechanisms include the lack of backlash, lack of non-linearity, simple monolithic structure, and ease of manufacturing. These advantages would enable ultra-high-precision positioning. Therefore, flexure mechanisms are suitable to be used for a nano-stage in the fields of biomedical science.

In some cases in the field of biomedical science, it is necessary for the stage to be designed as a hollow type with compact size for the measurement of biological specimens. Recently, in the field of ultra-precision microscopy for bio-nanotechnology, many combination AFM and confocal microscopes have been developed.^{4,5} Both upper- and underside of the stage of such combined microscopes should be accessible by the AFM tip and illuminated by the light of the objective lens. Therefore, the center of the stage should be hollow for light to reach the specimen. There are a lot of precision stages with PZT and flexure mechanisms; however, there are not many of the hollow type stage.

B. Review of previous research

Li and Xu presented a totally decoupled flexure based hollow type XY parallel micromanipulator, where the stage

has the working range of 124 μm . In order to reduce the effects of the temperature gradient, both the stages have quad symmetric structures.^{6,7} However, these stages do not have a rotational motion. They only have 2-degrees of freedom (DOF) (XY translational motion). Rotational motion is necessary to compensate for yaw error motion.

Several in-plane motion (3-DOF) flexure stages have been designed for a precision stage. Kang presented an ultra-precision $XY\theta_Z$ stage as a fine stage, where the design utilizes a plane mechanism and symmetric hexagonal structure that consists of a monolithic flexure hinge mechanism with three piezoelectric actuators and six flexures preserving the plane motion.⁸ Yong studied the effects of the accuracies of flexure hinge equations on the output compliances of micro-motion stages.⁹ However, these stages have no amplification mechanism, so the working range of the stage is very small. A major drawback of PZT arises from its small travel stroke. If the required working range is short, the amplification mechanism is not needed. However, if the required working range is long when compared to PZT performance, the amplification mechanism is essential.

Several amplification flexure mechanisms have been studied. Xu and Li researched a large output displacement amplification flexure mechanism.¹⁰ Hua designed a 3-DOF ($XY\theta_Z$) compliant micro positioning stage with an amplification mechanism, and performed an optimal design and input coupling analysis.¹ Tian presented the mechanical design and dynamics of a 3-DOF flexure stage with an amplification mechanism.¹¹ Aside from these, similar parallel mechanism stages were designed for many applications.¹²⁻¹⁵ In particular, several stages have double amplification mechanisms for longer working ranges.^{16,17} As aforementioned, in some case, a stage for the field of biomedical science is required to be a hollow type design.^{4,5} Light needs to be able to pass through a transparent biomedical cell specimen. Hollow stages are used in inverted microscopes for the measurement of

^{a)} Author to whom correspondence should be addressed. E-mail: gydud0717@kaist.ac.kr. Tel.: 82-42-350-3265. Fax: 82-42-350-5225.

transparent biomedical cell specimens. However, although all of the above 3-DOF stages have a sufficient working range, ultra-precision, and compact size, they are not hollow type stages. It is relatively easy to design a 2-DOF hollow type stage. However, in a 3-DOF parallel type stage, it is not easy to design a hollow type due to the triangular structure.

The conventional flexure-based linear compliant mechanism for the multi-axis ultra-precision motion can be classified as either serial or parallel. The serial compliant mechanism has disadvantages: the dynamic characteristics of one axis are different from those of the other axes, and positional errors produced by each axis are accumulated and contribute toward the error of the final axis. A parallel type mechanism is preferred over the serial mechanism. Chang presented a 3-DOF serial type stage. Chang's stage consists of two independent stages, which are the X-Y stage and the θ_z stage.^{18,19} In Chang's stage, the errors of the X-Y stage were propagated to the θ_z stage, so the total stage did not have ultra-precision performance. Therefore, the parallel type compliant mechanism is widely used in a 3-DOF precision stage. However, for a parallel type stage, the modeling and design of the flexure mechanism is complicated, and there are coupling motions, which bring about short working ranges compared to a serial type stage. Moreover, if the stage needs a hollow type design while maintaining a compact size, it is more difficult to arrange the PZT actuators and the flexure amplification mechanisms. In particular, the design of a compact amplification mechanism is difficult in the proposed stage. The design and modeling of various hinge lever mechanisms of an amplification device are presented for increasing small PZT actuator out range in references.²⁰⁻²² Many developed stages have amplification mechanisms.¹¹⁻¹⁶ In those studies, various design conditions, to achieve a higher magnification ratio, were considered. However, they are not suited for hollow type.

C. Feature of proposed stage

This paper discusses the mechanical design of a 3-DOF flexure-based parallel compliant mechanism for the hollow type biomedical specimen stage. Even though the proposed stage can be applied to both parallel compliant mechanisms and hollow types, the stage has a large working range and a nanometer resolution with compact size. Especially, the proposed stage has a double amplification flexure mechanism for a large working range. The proposed double amplification flexure mechanism was designed to provide effective spacing for a compact size. In short, the proposed stage has four important features: (1) hollow type; (2) 3-DOF in-plane motion; (3) large working range with double amplification mechanism in compact size; and (4) parallel compliant mechanism for high precision. There were no previous researches, which have reconciled the above four important features.

In this article, a positioning system developed by Kim *et al.* is extended to have a long working range and it is experimentally evaluated.²³ The rest of this paper is organized as follows: Sec. II introduces a conceptual 3-DOF stage design and double amplification design. In Sec. III, design of the amplification is discussed. In Sec. IV, modeling is dis-

cussed. In Sec. V, an optimization procedure is discussed. In Sec. VI, a measurement system and the experimental results are described. Conclusions are presented in Sec. VII.

II. CONCEPTUAL DESIGN

The main purpose of this novel stage is positioning of the specimen in relation to measurement equipment. For biological specimens in particular, the stage should sometimes be designed as a hollow type with a compact size. The central concept is that the mechanism should be the compliant equivalent of a conventional planar parallel 3-revolute-revolute-revolute. Since the PZT actuator has a limited deformation range of approximately $10 \mu\text{m/cm}$, a displacement amplification mechanism is usually integrated with a PZT actuator in the stage to achieve motion ranges up to hundreds of micrometers. The biggest problem is that the stage of the hollow type has very tight space restrictions. Both the PZT actuator and the amplification mechanism should be inside the small stage. At the same time, the stage should be designed to attain a motion range of $\pm 100 \mu\text{m}$ in the X and Y directions, and $\pm 0.1^\circ$ in the θ_z direction. In addition, the diameter of the center hole should be greater than 60 mm. Therefore, except for this center hole, in this study, the three PZT actuators and three amplification mechanisms were placed on the compact stage. The schematic model of the 3-DOF in-plane mechanism is shown in Fig. 1. For compactness, the proposed amplification mechanism has two important characteristics. First, the PZT actuator is embedded in the amplification mechanism. Because the amplification mechanism consists of an L-shape lever mechanism, the PZT actuator can be assembled easily in the remaining space of the L-shape lever. Second, the proposed amplification mechanism uses a double amplification mechanism, which has two L-shape levers for one amplification device. The proposed double amplification mechanism has the merit

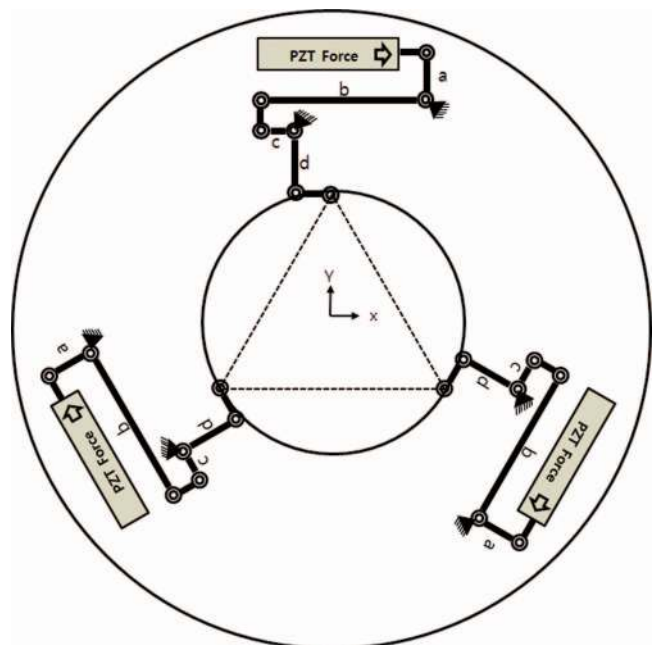


FIG. 1. Schematic model of 3-DOF stage.

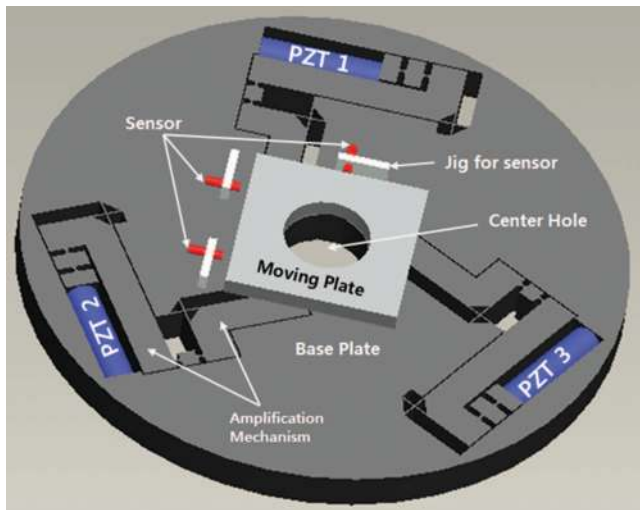


FIG. 2. Schematic illustration of proposed stage.

of compactness and does not block the center hole. In addition, the double amplification mechanism efficiently amplifies the motion output by using two levers. Therefore, the motion amplification ratio is $(b/a) \times (d/c)$ at Fig. 1. The whole system simply consists of the base plate, which includes three PZT actuators and hinge amplification mechanisms, and a moving plate, which is set on the ends of the three amplification mechanisms. Additionally, three capacitive sensors, which are used to measure the in-plane motion of the moving plate, are attached on the base plate for closed loop control. Figure 2 presents a schematic illustration of the proposed concept design.

III. AMPLIFICATION MECHANISM DESIGN

The proposed amplification mechanism plays the role of motion guide and displacement amplification in the nano-motion stage. Figure 3 presents a developed amplification mechanism that consists of two L-shape levers, circular hinges, and a cartwheel hinge.

A circular hinge which is precise in rotation has been most widely used in precision PZT stages,^{24–26} and a cartwheel hinge, which is a kind of compound flexure hinge, is one of the most popular elements because of its larger oper-

ational displacement.^{27–29} An amplification process is as follows. A displacement of the PZT actuator is amplified by the first L-shape lever mechanism, which is expressed as rigid body 3. The rigid body 4, which has amplified displacement by the first L-shape lever mechanism, applies the force at the second L-shape lever mechanism, which is expressed as rigid body 5. Therefore, a displacement of rigid body 4 is amplified by the second L-shape lever mechanism, like the displacement of a PZT actuator, which is amplified by the first L-shape lever mechanism. If the motion amplification ratio of the first lever is b/a , and the motion amplification ratio of the second lever is d/c , then rigid body 19, which is joined to the moving plate, is amplified by amplification ratio $(b/a) \times (d/c)$. However, the use of lever mechanisms in a flexure based system leads to “lost motion” situations, due to lever hinge stretching. The simulation results of lost motion are represented in Table I. The theoretical amplification ratio is 5, but the simulation result is 4. The 20% of the motion was lost by lost motion effect. Therefore, lost motion is an important factor in amplification mechanism design. To calculate “lost motion” from flexure hinge stretching, the stretching should be modeled in the design equations of the levers. The modeling of the hinge is represented in Sec. IV.

Another important factor in amplification mechanism design is stress. Three rigid bodies 2, 4, and 6 are the connecting bodies, which reduce the maximum stress of the hinge. For example, the L-shape lever mechanism has a curvilinear motion, while the displacement of the PZT actuator is a rectilinear motion. If there were no rigid body 2, only one flexure hinge would play the role of a rotational joint. This can lead to material failures; besides, the force of the PZT actuator is not transferred vertically at the end of the L-shape lever mechanism. In other words, rigid body 2 is a kind of buffer. Two flexure hinges ① and ② share the stress concentrated by the connecting rigid body 2. The other connecting bodies “4” and “6” are based on the same principle. However, even though the amplification mechanism has these connecting bodies, the places, which have a large rotational motion, make problems of material failures. The flexure hinges ⑦ and ⑧, which are at the end of the amplification mechanism, have the largest rotational motion. The flexure hinges ③ and ⑥, which are fixed to the base plate, have a large rotational motion. Points like these hinges are dangerous, due to the potential for material failures. Therefore, cartwheel hinges, which have a larger

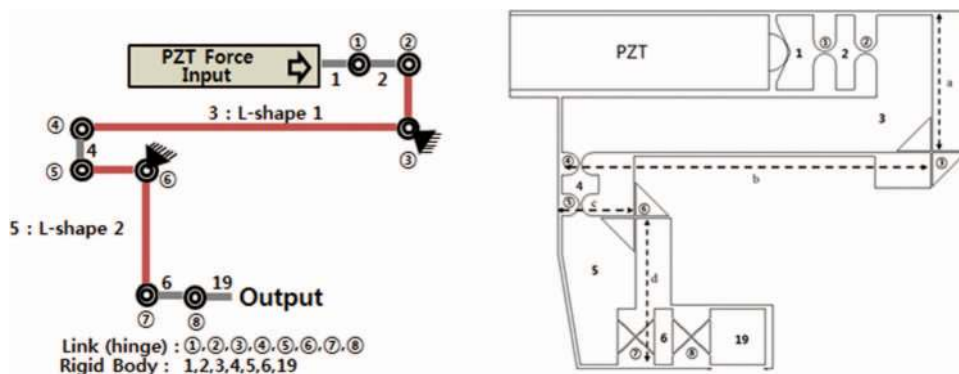


FIG. 3. Developed amplification mechanism.

TABLE I. Lost motion.

Simulation parameters	a = 35 mm	b = 100 mm	c = 20 mm	d = 35 mm
Actuating force at body 1	5 N	10 N	15 N	20 N
Displacement of body 1	2.82 μm	5.65 μm	8.53 μm	11.32 μm
Displacement of body 19	11.56 μm	22.15 μm	34.12 μm	45.21 μm
FEM amplification ratio	4.09	3.92	4.0	3.99
Theoretical amplification ratio	$(b/a) \times (d/c) = 5$			

operational displacement, are used at dangerous points. In order to verify the large displacement of the cartwheel hinge, FEM simulation of the comparison between the circular hinge and cartwheel hinge was performed under the same dimensional condition. The performance of the flexure hinge mechanism is heavily influenced by the hinge thickness, the hinge radius, the hinge width, and the hinge length. Therefore, the simulation was conducted by various parameters. However, because the amplification mechanism must be inside the small stage, the area of the hinge was no larger than 20 mm \times 20 mm. Figure 4 presents simulation parameters. Both hinges had the same hinge width of $b = 20$ mm, the cartwheel hinge height equals the circular hinge diameter for the same area condition, and the actuated force was 5 N.

Simulations were carried out for various hinge thicknesses and various hinge radii. Simulation results were represented in Figs. 5–7. The simulation indicated that a cartwheel hinge has better performance than a circular hinge for the same constraints. Figure 5 presents the rotational displacement of both flexure hinges when the same force (5 N from Fig. 4) is applied for various hinge thicknesses and various hinge radii. As expected, the cartwheel hinge has a longer displacement than the circular hinge when the hinge is thin. In a flexure mechanism, a large rotational displacement causes excessive stress, and the excessive stress creates the possibil-

ity of material failure. Figure 5 shows the hinge displacement and Fig. 6 shows the hinge stress when the hinges were deformed by Fig. 5. As shown in Fig. 6, although the cartwheel hinge has a longer displacement than the circular hinge for same input force, the stress of the cartwheel hinge is similar to the stress of the circular hinge. Considering material yield strength, these results indicate that the cartwheel hinge is better than the circular hinge because longer displacement and less stress are better for the amplification mechanism. Figure 7 shows the rotational displacement per unit stress (divide Fig. 5 into Fig. 6). As shown in Fig. 7, the cartwheel hinge has better performance. However, the cartwheel hinge is much more difficult to manufacture, and the price of manufacturing is quite expensive. Also, the dynamic characteristics, like a fast response and robustness against several dynamic disturbances, get worse because the bandwidth of the total system goes down. To overcome these disadvantages, an optimal design process is required.

IV. MODELING

In order to optimize the flexure mechanism, a static and a dynamic model of the stage must be established first. The proposed $XY\theta_Z$ stage can be modelled as a multi spring-multi

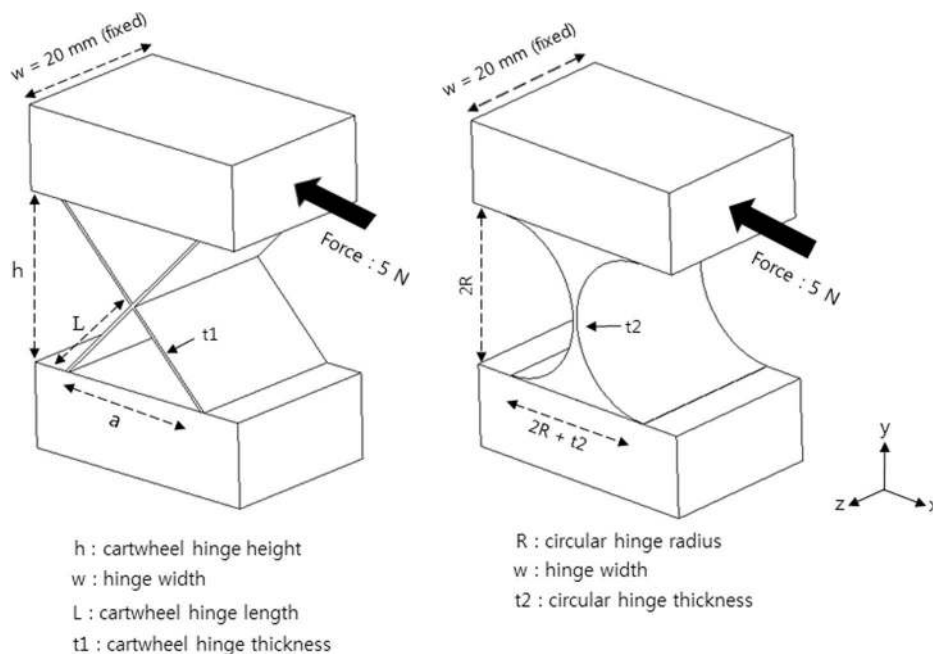


FIG. 4. Hinge parameters.

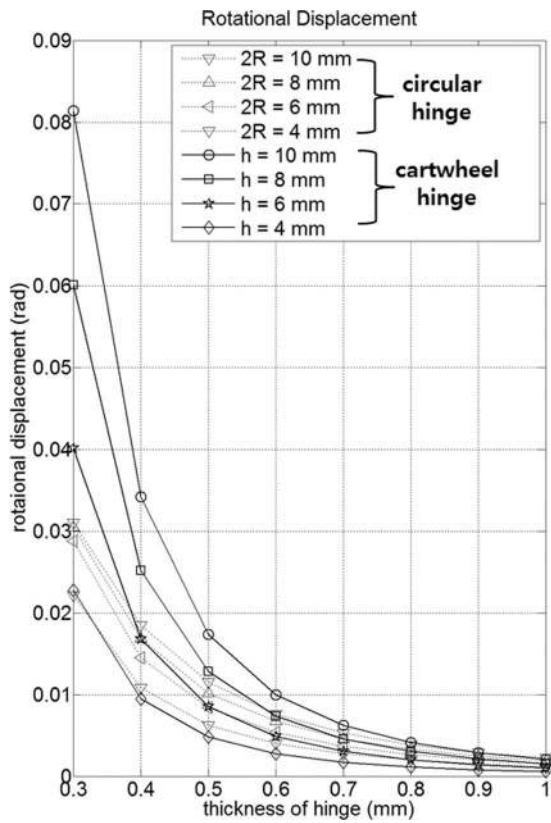


FIG. 5. Comparison of rotational displacement between circular hinge and cartwheel hinge.

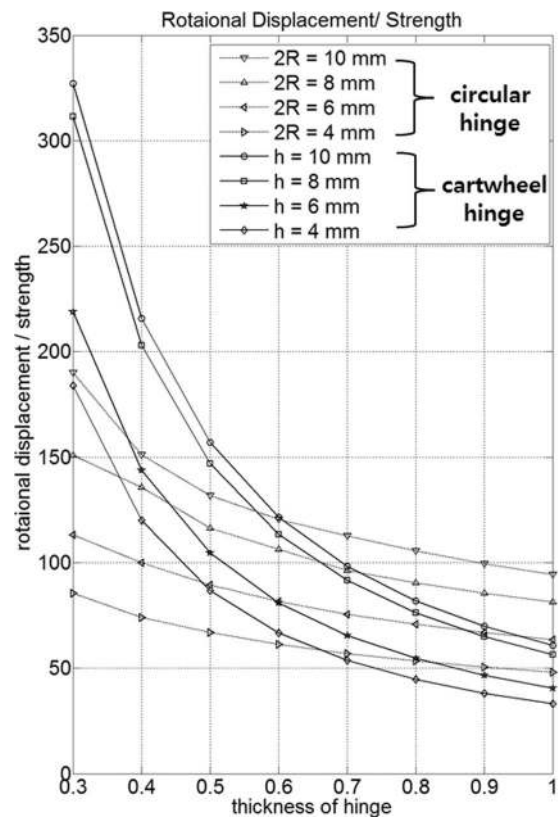


FIG. 7. Comparison of "displacement/stress" between circular hinge and cartwheel hinge.

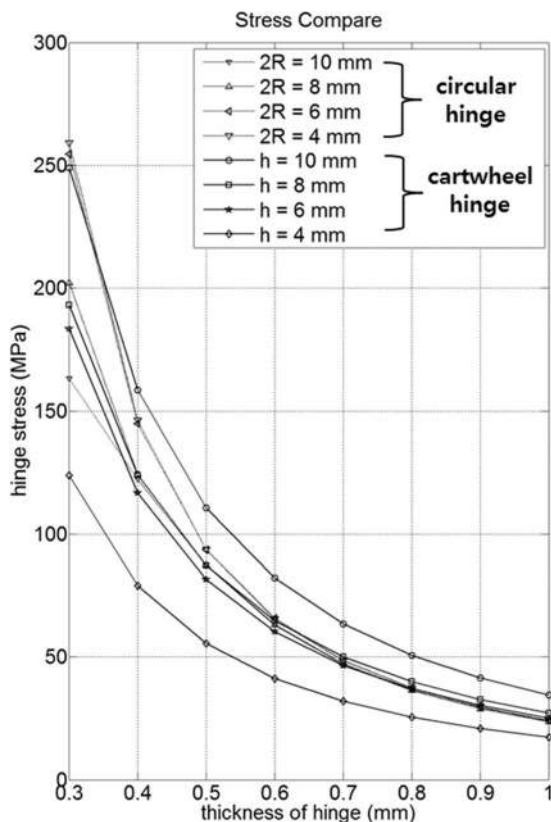


FIG. 6. Comparison of maximum stress between circular hinge and cartwheel hinge.

mass system. The flexure hinge is regarded as a spring with six-directional stiffness, and the rigid body is regarded as a dumped mass without any elasticity. The stage consists of 24 flexure hinges and 19 rigid bodies. The spring-mass system is modeled by Ryu's method.^{16,30} This method requires 6×6 stiffness matrices of all the springs. Equation (1), compliance equation, shows the displacement of the tip of the general hinge when external forces are exerted on it. The lost motion in Sec. III is calculated by Eq. (1). Therefore, more accurate 6×6 stiffness matrices can calculate the amplification motion displacement

$$\begin{pmatrix} \delta_x \\ \delta_y \\ \delta_z \\ \delta_\alpha \\ \delta_\beta \\ \delta_\gamma \end{pmatrix} = \begin{pmatrix} c1 & 0 & 0 & 0 & c3 & 0 \\ 0 & c2 & 0 & -c4 & 0 & 0 \\ 0 & 0 & c5 & 0 & 0 & 0 \\ 0 & -c4 & 0 & c6 & 0 & 0 \\ c3 & 0 & 0 & 0 & c7 & 0 \\ 0 & 0 & 0 & 0 & 0 & c8 \end{pmatrix} \begin{pmatrix} F_x \\ F_y \\ F_z \\ M_x \\ M_y \\ M_z \end{pmatrix} \quad (1)$$

As mentioned earlier, two kinds of hinges, the cartwheel hinge and the circular hinge, are used in the proposed stage. Both flexure hinges have been widely used in the precision PZT stage. There have been many methods adopted to derive satisfactory compliance equations of these two hinges. The matrix of stiffness with these two hinges has been intensively studied. Koseki made a stiffness matrix of a circular hinge easily.²⁵ Kang calculated the stiffness of the cartwheel

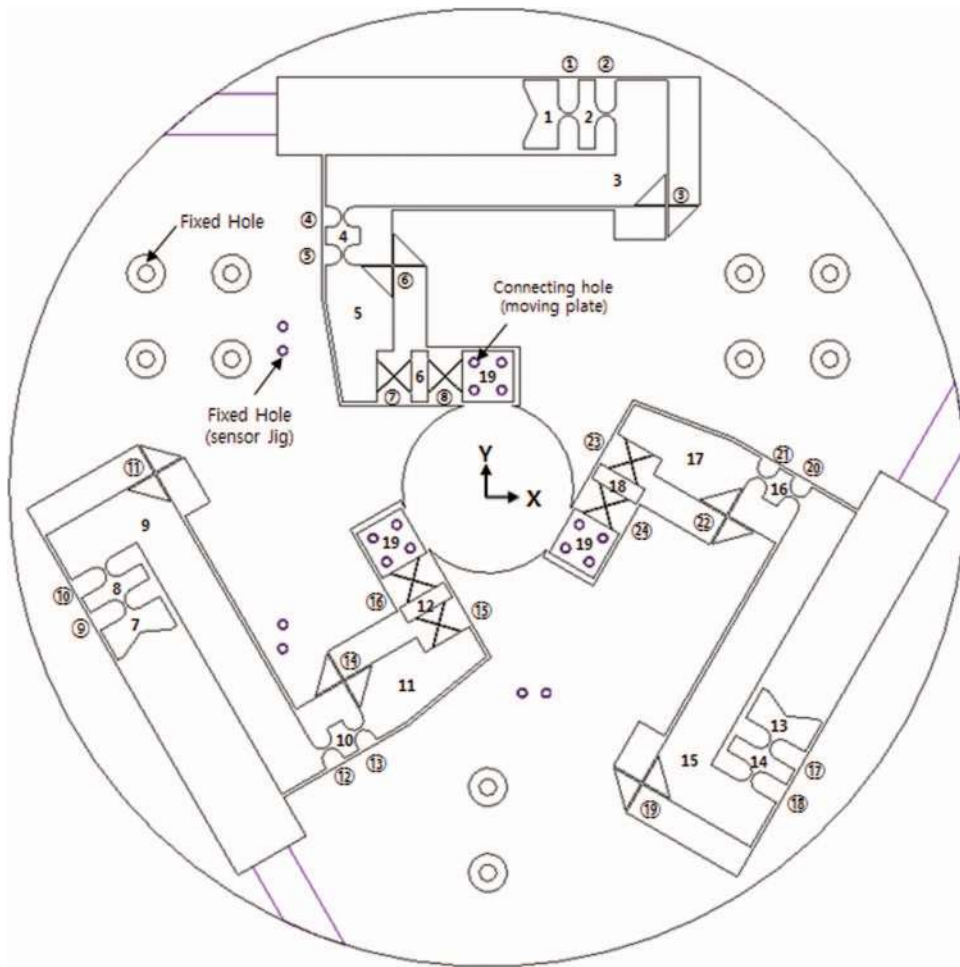


FIG. 8. Developed 3-DOF compliant mechanism.

hinge using four general leaf springs and an imaginary body.³¹ Using the stiffness matrices from these two references,^{25,31} the whole flexure mechanism is modeled as rigid bodies connected through a hinge spring. There are 12 cartwheel hinges, 12 circular hinges, and 19 rigid bodies in the whole positioning system (see Fig. 8).

Using Ryu’s method, the displacement of all bodies and stresses at all hinges were calculated for given input displacements or external force. Our analytic model is briefly presented in this paper. From Ryu’s modeling method,¹⁶ the following equation is obtained:

$$M\ddot{x} + Kx = F, \tag{2}$$

where

$$M = \begin{bmatrix} M^1 & & 0 \\ & \ddots & \\ 0 & & M^{N_b} \end{bmatrix}_{6N_b \times 6N_b}, \tag{3}$$

$$M^i = [m^i \quad m^i \quad m^i \quad I_x^i \quad I_y^i \quad I_z^i], \tag{4}$$

$$K = \begin{bmatrix} K_{11} & \cdots & K_{1N_b} \\ \vdots & \ddots & \vdots \\ K_{N_b1} & \cdots & K_{N_bN_b} \end{bmatrix}_{6N_b \times 6N_b}, \tag{5}$$

$$K_{ij} = \begin{cases} \sum_{k=1}^{N_h} T_k^{iT} k_k T_k^i, & \text{for } i = j \\ -T_k^{iT} k_k T_k^i, & \text{for } i \neq j \end{cases}, \tag{6}$$

$$F = [f^1 \quad \cdots \quad f^{N_b}]_{6N_b \times 1}^T, \tag{7}$$

$$x = [q^1 \quad \cdots \quad q^{N_b}]_{6N_b \times 1}^T, \tag{8}$$

$$q_i = [x^i, y^i, z^i, \theta_x^i, \theta_y^i, \theta_z^i]^T. \tag{9}$$

In Eqs. (3)–(9), N_b and N_h represent the number of bodies and the number of hinges, respectively. And m^i is the mass of body i , and I_x^i , I_y^i , and I_z^i are the moments of inertia with respect to the local coordinate systems fixed to body i . For the geometric model of our mechanism, 19 bodies and 24

TABLE II. Stiffness verification of the 3-DOF stage.

	Analytic model	FEM simulation	Error
K_x	0.102 N/ μ m	0.111 N/ μ m	8.1%
K_y	0.106 N/ μ m	0.112 N/ μ m	5.3%
K_z	5.026 N/ μ m	5.263 N/ μ m	4.5%
K_{θ_x}	5625.4 Nm/rad	5837.1 Nm/rad	3.6%
K_{θ_y}	5845.2 Nm/rad	6164.4 Nm/rad	5.2%
K_{θ_z}	173.1 Nm/rad	189.4 Nm/rad	8.6%

hinges were used. Because each body has 6-degrees of freedom (Eq. (9)), the size of the x vector is $|(6 \times 19) \times 1|$. Similarly, the force vector F also has the same size $|114 \times 1|$. The system mass matrix M and the system matrix K have the size of $|(6 \times 19) \times (6 \times 19)|(|114 \times 114|)$. Finally, if we ignored the second-order term in Eq. (2), the static displacements of all bodies can be calculated from the total stiffness matrix (Eq. (5)) and the input force vector (Eq. (7)):

$$Kx = F. \quad (10)$$

Therefore, we can know that the displacements of all rigid bodies for given input displacements or external forces. For example, in Fig. 8, if the input force or displacements are applied at rigid bodies (1,7,13), then we will be able to know 6-degree of freedom displacements of all 19 rigid bodies. The stiffness values of the analytic model are compared with FEM simulation results. The parameters of the hinge joint are that L is 8 mm, t_1 is 0.5 mm, and r is 3 mm, t_2 is 0.6 mm, and b is 25 mm (refer to Fig. 4). The modeling of the whole stage shows a reasonable prediction of stiffness with errors less than 15% (see Table II). Results of the analytic model in Table II were obtained by Eq. (10). For example, to obtain X-direction stiffness, X-direction force (1 N) was applied to the moving plate (rigid body number (19), see Figs. 2 and 8),

$$Kx = [f^{1T}, f^{1T}, \dots, f^{N_b^T}]^T, \quad (11)$$

where

$$f^{19} = [1N, 0, 0, 0, 0, 0]^T$$

$$f^i = [0, 0, 0, 0, 0, 0]^T, \quad i = 1, 2, 3, \dots, 18. \quad (12)$$

If we can know the displacement of the moving plate in the X-direction analytically, then the X-stiffness of the system can be obtained. The stiffness of the system for the other directions can be obtained using the same approach. FEM simula-

TABLE III. Verification of natural frequency.

	Analytic model	FEM simulation	Error
Mode 1 (rotation)	235 Hz	221 Hz	6.7%
Mode 2 (translation 1)	251 Hz	226 Hz	11%
Mode 3 (translation 2)	252 Hz	230 Hz	9%

tion data were obtained by the Pro/Engineer-Mechanica tool. The multi-pass adaptive method was used, and the polynomial order is eight.

The all natural frequency is also calculated via Eq. (2). All of the structural natural frequencies of the system can be calculated from the mass and stiffness of the system solving the following eigenvalue problem:

$$[\mathbf{K} - \omega^2 \mathbf{M}] = 0, \quad (13)$$

where ω is a set of eigenvalues that represent modal frequencies.

The positive square root of the roots of Eq. (13) are the natural frequencies of the system.^{8,30}

The natural frequency verification results via FEM presented in Table III and Fig. 9 show the mode shapes of the lower three modes.

V. OPTIMAL DESIGN

Since the performance of the system is heavily influenced by the design parameters, an optimization procedure was performed to obtain the optimal design parameters. The model of the whole system presented in previous sections provides the basis for understanding the effects of such design parameters as hinge radius, width, thickness, and length. Because the relationship between the design parameters and the model performance is complicated, it is very difficult to determine the optimal design parameters manually. For the solution, a sequential quadratic programming (SQP) method and MATLAB have been used. The objective of the optimization procedure is to maximize the system bandwidth for improving the dynamic characteristics. Doing so can result in fast response and robustness against several dynamic disturbances. The following objective function is used:

$$\text{Minimize} \left(\frac{1}{\omega_{n,1}} \right)^2. \quad (14)$$

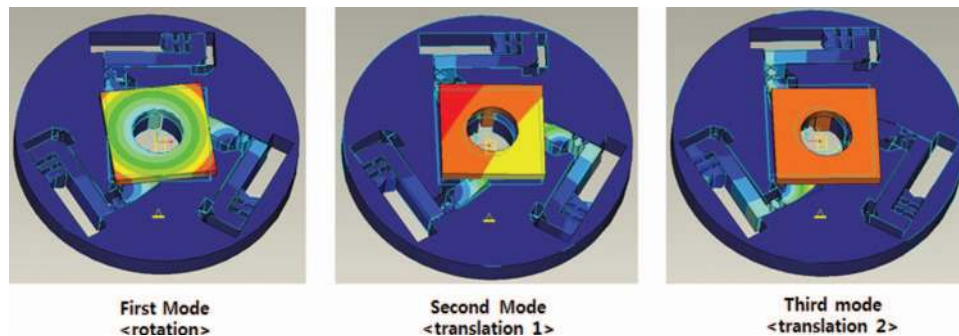


FIG. 9. FEM simulation of mode shape.

TABLE IV. Optimal design results.

Symbol	Design variables	Design range (mm)	Design variable sets							
			Start point					Optimum and design values		
			S ₁	S ₂	S ₃	S ₃	S ₅	S _{opt}	S _{design}	
L	Cartwheel hinge	Length of leaf-spring	$5 \leq L \leq 10$	5	6	7	10	9	8.13	8
t ₁		Thickness of leaf-spring	$0.3 \leq t_1 \leq 1$	0.4	0.6	0.3	0.9	0.8	0.51	0.5
R	Circular hinge	Radius of circular hinge	$1 \leq R \leq 10$	4	6	5	7	2	2.98	3
t ₂		Thickness of circular hinge	$0.3 \leq t_2 \leq 1$	0.9	0.2	0.5	0.6	0.1	0.62	0.6
w	Width of cartwheel and circular hinge		$10 \leq w \leq 30$	12	16	28	23	19	24.82	25
a	Lever 1	Length of short side	$20 \leq a \leq 40$	31	25	26	34	21	36.84	37
b		Length of long side	$80 \leq b \leq 120$	93	105	107	117	82	99.62	100
c	Lever 2	Length of short side	$10 \leq c \leq 25$	24	15	11	22	19	19.12	20
d		Length of long side	$30 \leq d \leq 50$	42	39	32	35	45	40.12	40

There are nine design parameters, all of which are presented in Figs. 3 and 4. More specifically, L , t_1 relate to the cartwheel hinge, r , t_2 relate to the circular hinge, w relates to the common hinge width, and a , b , c , d relate to the L-shape levers. The other parameters like the size of the rigid bodies do not significantly affect the system performance. Therefore, these parameter values were set as constants. The optimization problem includes a number of constraints to satisfy several specifications. There are many constraints in this optimal problem. The first are the constraints related to workspace. When the moving plate (rigid body 19) is in maximum pose, the stroke of the rigid bodies (1, 7, 13), which are in contact with actuators, is smaller than the maximum deformation of the actuators. The specification of the workspace is ± 100 μm in the X and Y directions and $\pm 0.1^\circ$ in the θ_z direction, respectively. Considering the factor of safety, the workspace is ± 120 μm in the X and Y directions and $\pm 0.12^\circ$ in the θ_z direction. Therefore, the constraints of the workspace are as follows:

$$g_i = \delta_{\text{rigid_body}_j} - \delta_{\text{max_PZT_performance}} < 0$$

$$(i = 1, 2, 3, \quad j = 1, 7, 13). \quad (15)$$

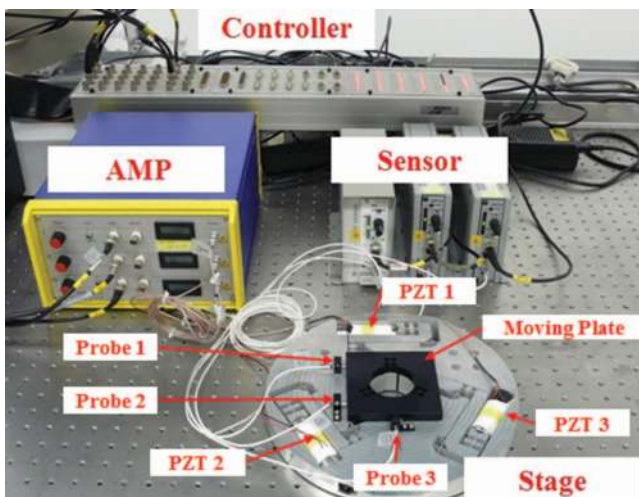


FIG. 10. Hardware components.

The force of the actuator should also be considered. Because of the high stiffness of the stage, the deformation of the PZT actuator does not work unexpectedly. Therefore, both the stiffness of the PZT actuator and the stiffness of the flexure mechanism should be considered for the constraints,

$$g_i = S_f \times \delta_{\text{rigid_body}_j} - (\delta_{\text{max_PZT_performance}})$$

$$\times \frac{K_{\text{PZT_stiffness}}}{K_{\text{PZT_stiffness}} + K_{\text{flexure_stiffness}}} < 0$$

$$(i = 4, 5, 6, \quad j = 1, 7, 13). \quad (16)$$

To guarantee a fast response and robustness against several dynamic disturbances, the first natural frequency should be higher than at least 80 Hz,

$$g_7 = 80 - f_{n,1} < 0. \quad (17)$$

Next, the maximum stress constraint should be considered. The maximum stress occurs at the hinge when the rotational displacement of the hinge is at the maximum value. The maximum stress of the circular hinge is given by Ref. 16.

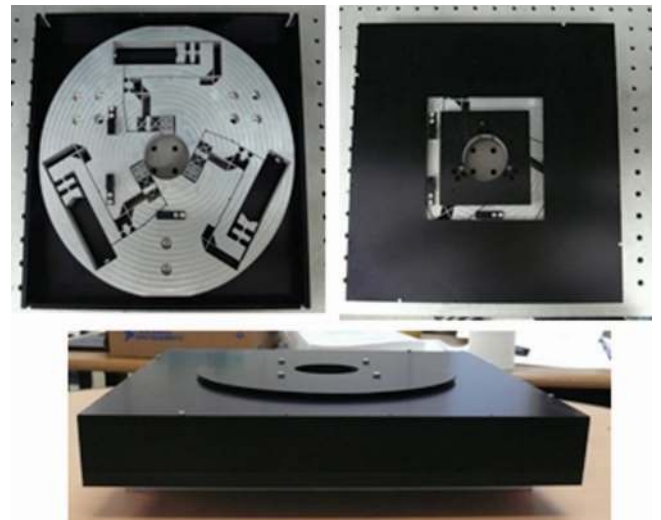


FIG. 11. Developed 3-DOF stage with case.

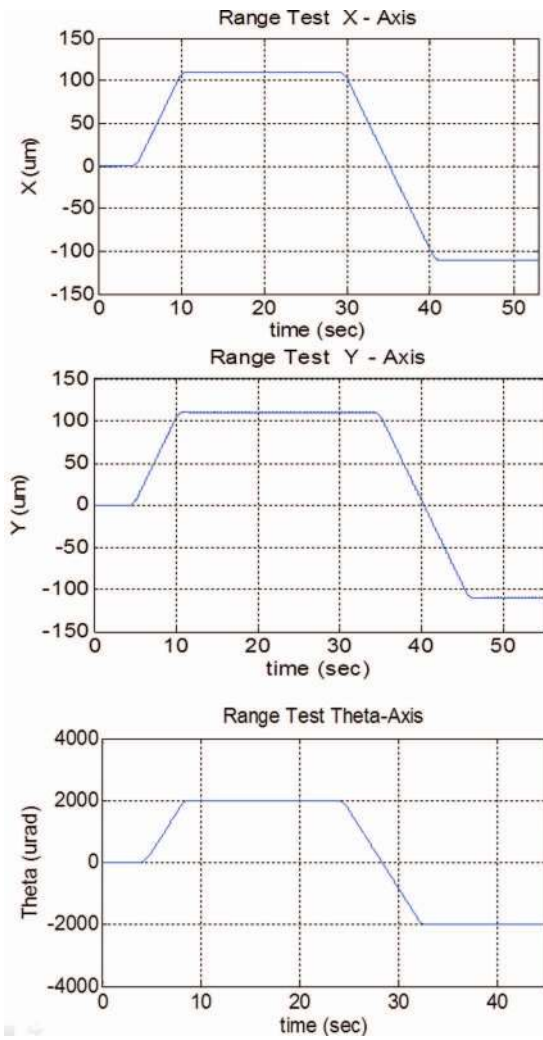


FIG. 12. Experiment results of range test.

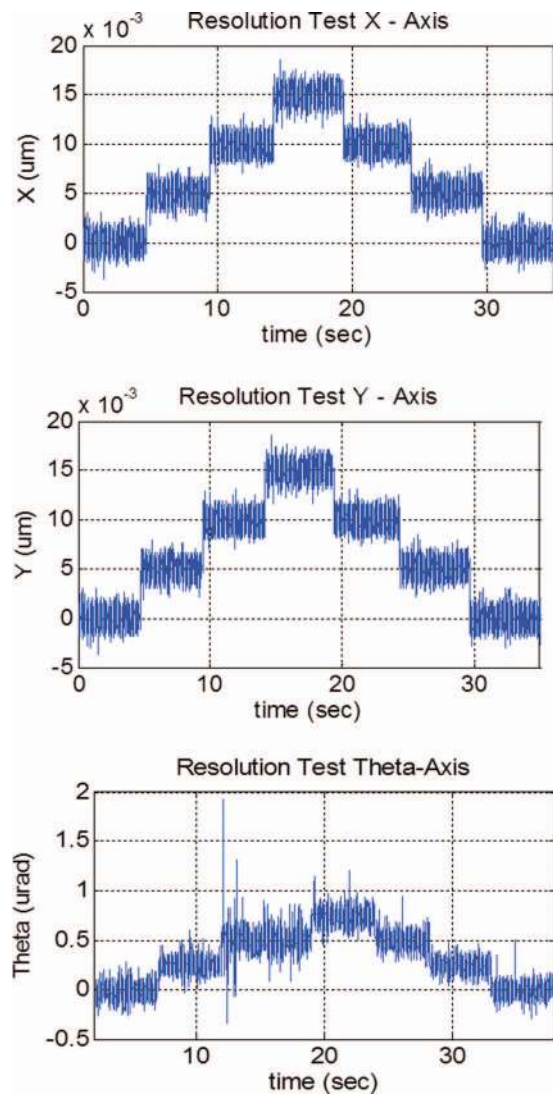


FIG. 13. Experiment results of resolution test.

First, a circular hinge of one amplification is considered:

$$g_j = S_f |\theta_z^i - \theta_z^{i+1}| - \frac{t_{2i}^2 b}{6K_i^i} \times \sigma_Y < 0 \quad (j = 8, 9, 10, 11). \tag{18}$$

The stress of the cartwheel hinge is considered. The maximum stress of the cartwheel hinge is given by Ref. 24:

$$g_i = S_f |\theta_z^i - \theta_z^{i+1}| - \frac{L}{Et_{1i}} \times \sigma_Y < 0 \quad (i = 12, 13, 14, 15). \tag{19}$$

The constraints of hinge size are then considered:

$$g_{16} = R - 5t_2 < 0, \tag{20}$$

$$g_{17} = t_2 - R < 0. \tag{21}$$

Finally, the constraints of the stiffness of the rigid bodies are considered. The stiffness of the rigid bodies (3, 9, 15) are restricted to ten times higher than the stiffness of the total flexure mechanism. This constraint is that bodies are regarded as rigid bodies:

$$g_{18} = 10 \times k_{movingpart} - k_{rigid_body(beam)} < 0. \tag{22}$$

The SQP method does not guarantee that it will always yield a global minimum. In this study, five different starting points were used, all of which yielded the same minimum value to verify that the global minimum had been found. The results of the optimization are given in Table IV, with the first natural

TABLE V. Performance of stage with optimal design.

	Analytic model (optimum values)	FEM (optimum values)	FEM (design values)
Max displacement (X- direction)	238 μm	228 μm	228 μm
Max displacement (Y- direction)	229 μm	225 μm	225 μm
Max displacement (θ_z - direction)	0.23°	0.23°	0.23°
Mode 1 (rotation)	88.24 Hz	89.91 Hz	88.11 Hz
Mode 2 (X - translation)	98.34 Hz	94.53 Hz	94.32 Hz
Mode 3 (Y - translation)	99.21 Hz	95.12 Hz	95.48 Hz

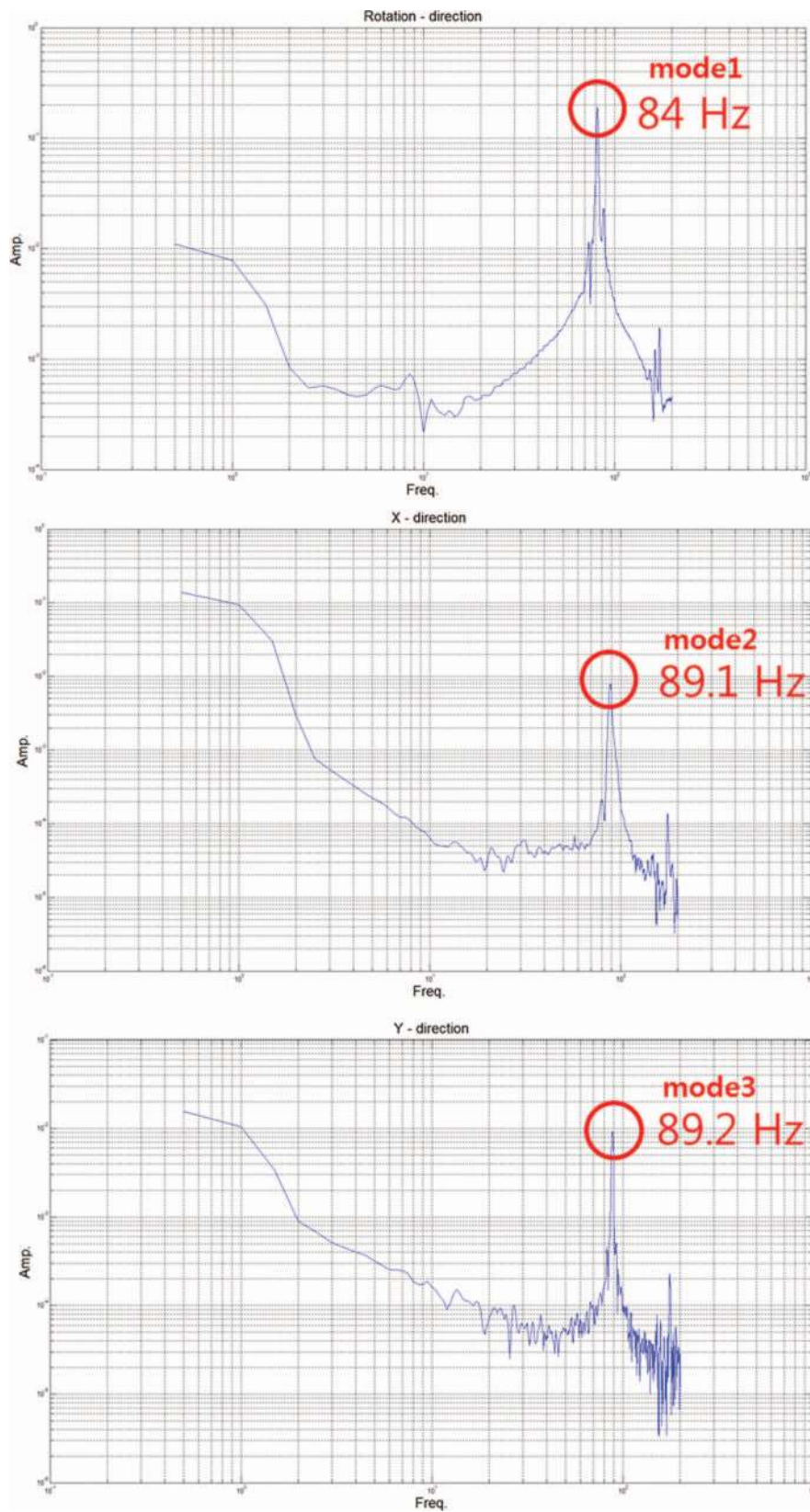


FIG. 14. Experiment results of first three mode test.

frequency being 89 Hz and the maximum range of translation motion being $228 \mu\text{m}$ (Table V). When considering the precision of the manufacturing machine, the optimum value cannot be used. The reasonable design values were used in

the proposed positioning system. There is little difference in performance between the optimum values and design values. The stage performance is fully satisfied compared with the FEM simulation results.

VI. EXPERIMENT AND RESULTS

The proposed stage can be manufactured from a single monolithic piece via wire electro discharge machining (WEDM), therefore reducing the problems associated with assembly. The material was used Al7076 T6 whose yield strength is 506 MPa. After manufacturing, the stage was integrated with PZT actuators (Pst 1000/25/60) produced by Piezomechanik GmbH. The controller was DS1103 (dSPACE corp.), the amplifier to drive the PZT actuators was SVR 1000-3 (Piezomechanik GmbH.), and the capacitor sensors were three CPL190 (Lion Precision). These sensors have 4.5 nm resolution at 100 Hz. These sensors were attached by three sensor jigs and measured X, Y, and θ_z directional displacements of the moving plate. Using these three displacement sensors and proportional integral differential control algorithm, the stage was controlled in the 3-axis. Figure 10 shows the hardware components of the system and Fig. 11 shows the final system with the case. The size of the total system is 290 mm \times 290 mm \times 30 mm, and the diameter of the center hole is 55 mm. To test the load capacity, a block of 2 kg was placed on the stage. The experimental results are presented in Figs. 12 and 13. The stroke of the translational movement was 220 μ m, and the stroke of the rotational movement was 0.22 $^\circ$, whereas their in-position stabilities were ± 2 nm and ± 30 nrad, respectively, and their resolutions were 5 nm and 0.25 μ rad, respectively. The settling time is below 50 ms. In-position stability means a holding accuracy or noise band at stop state. The developed stage has larger working range than other 3-DOF stages (Ref. 12–17). Also, the size of the stage is compact even though the stage has a center hole. Compared to Table IV, the stroke of the stage greatly agreed with FEM simulation results in all three axes. Figure 14 represents experimental results of the first three mode test. The result shows a reasonable prediction of the first three modes with errors less than 10%. The main cause of the difference between the experiment results and simulation results is the error of the manufacturing process. In particular, in the manufacturing process, the cartwheel hinge could not have an exact radius of a fillet at the center of the hinge or at the end of the hinge because the minimum diameter of the wire available with WEDM is 20 μ m. Even if the stage has small errors, the original goals were achieved because of enough margin from the designed factor of safety.

VII. CONCLUSIONS

A novel XY θ_z -stage, designed to have the center hole as well as long working range, was proposed. To achieve a long working range, a novel double amplification mechanism, with a cartwheel hinge, was developed. The optimization procedure, to determine the parameters that would optimize the design of the stage, was performed. Based on the optimal design parameters, the system was manufactured and tested for the verification of the system. Experimental results demonstrated

the performance of the ultra-precision stage. The stroke of the translational movement was ± 110 μ m, and the stroke of the rotational movement was $\pm 0.11^\circ$. The resolutions were 5 nm and 0.25 μ rad, respectively. Future research directions include use of the stage for the measurement of biological specimens with high resolution microscope equipment.

ACKNOWLEDGMENTS

This research was supported by WCU (World Class University) program through the National Research Foundation of Korea funded by the Ministry of Education, Science and Technology (R31-2008-000-10045-0).

- ¹H. Wang and X. Zhang, *Mech. Mach. Theory* **43**(4), 400–410 (2008).
- ²Y. Li and Q. Xu, *J. Intell. Robotic Syst.* **55**(4), 377–402 (2009).
- ³L. Yangmin and X. Qingsong, *IEEE Trans. Autom. Sci. Eng.* **8**(2), 265–279 (2011).
- ⁴Y. D. Suh, G. K. Schenter, L. Zhu, and H. P. Lu, *Ultramicroscopy* **97**(1–4), 89–102 (2003).
- ⁵R. Kassies, K. O. Van Der Werf, A. Lenferink, C. N. Hunter, J. D. Olsen, V. Subramaniam, and C. Otto, *J. Microsc.* **217**(1), 109–116 (2005).
- ⁶Y. Li and Q. Xu, *Mech. Mach. Theory* **44**(12), 2127–2152 (2009).
- ⁷L. Yangmin and X. Qingsong, *IEEE Trans. Rob.* **25**(3), 645–657 (2009).
- ⁸D. Kang, K. Kim, Y. Choi, D. Gweon, S. Lee, and M. Lee, *J. Mech. Sci. Technol.* **19**(11), 2157–2164 (2005).
- ⁹Y. K. Yong and T.-F. Lu, *Mech. Mach. Theory* **43**(3), 347–363 (2008).
- ¹⁰Q. Xu and Y. Li, *Mech. Mach. Theory* **46**(2), 183–200 (2011).
- ¹¹Y. Tian, B. Shirinzadeh, and D. Zhang, *Microelectron. Eng.* **87**(2), 230–241 (2010).
- ¹²Y. Byung-Ju, C. Goo Bong, N. Heung Yeol, K. Whee Kuk, and S. Il Hong, *IEEE Trans. Rob. Autom.* **19**(4), 604–612 (2003).
- ¹³K.-B. Choi, *J. Mech. Sci. Technol.* **17**(4), 528–537 (2003).
- ¹⁴C. Wen Jie, L. Wei, K. H. Low, and Y. Guilin, in *Proceedings of the 2005 IEEE/ASME International Conference on Advanced Intelligent Mechatronics* (IEEE, 2005).
- ¹⁵Q. Yao, J. Dong, and P. M. Ferreira, *Precis. Eng.* **32**(1), 7–19 (2008).
- ¹⁶J. W. Ryu, Ph.D. dissertation, KAIST, 1997, pp. 70–71.
- ¹⁷K. Hu, J. H. Kim, J. Schmiedeler, and C.-H. Menq, *Rev. Sci. Instrum.* **79**(2), 025105 (2008).
- ¹⁸C. Shuo Hung, T. Chung Kai, and C. Hon Chan, *IEEE Trans. Ultrason., Ferroelectr., Freq. Control* **46**(4), 897–905 (1999).
- ¹⁹C. Shuo Hung, T. Chung Kai, and C. Hon Chan, *IEEE Trans. Ultrason., Ferroelectr., Freq. Control* **46**(4), 906–912 (1999).
- ²⁰M. Jouaneh and R. Yang, *Precis. Eng.* **27**(4), 407–418 (2003).
- ²¹E. Hwang, K. Min, S. Song, I. Ahn, and W. Choi, *J. Mech. Sci. Technol.* **21**(4), 616–623 (2007).
- ²²K.-B. Choi, J. J. Lee, and S. Hata, *Sens. Actuators, A* **161**(1–2), 173–181 (2010).
- ²³H.-Y. Kim, D.-H. Ahn, B.-S. Chun, and D.-G. Gweon, in *10th Proceedings of the IEEE Conference on Nanotechnology* (2010), pp. 903–906.
- ²⁴S. T. Smith, *Flexures* (Gordon and Breach, 2000), pp. 177–192.
- ²⁵Y. Koseki, T. Tanikawa, N. Koyachi, and T. Arai, *Adv. Rob.* **16**, 251–264 (2002).
- ²⁶Y. K. Yong, T.-F. Lu, and D. C. Handley, *Precis. Eng.* **32**(2), 63–70 (2008).
- ²⁷C. Kee-Bong, L. Jae Jong, and K. Min Young, in *Proceedings of the 2007 International Conference on the Control, Automation and Systems* (IEEE, 2007).
- ²⁸B. Shusheng, Z. Hongzhe, and Y. Jingjun, *J. Mech. Des.* **131**(6), 061010 (2009).
- ²⁹X. Pei, J. Yu, G. Zong, S. Bi, and H. Su, *Mech. Mach. Theory* **44**(10), 1900–1909 (2009).
- ³⁰J. W. Ryu, D.-G. Gweon, and K. S. Moon, *Precis. Eng.* **21**(1), 18–28 (1997).
- ³¹D. Kang, Ph.D. dissertation, KAIST, 2007, pp. 100–105.